Inorganic Chemistry

Article

pubs.acs.org/IC

Neutron Diffraction Study of Unusual Phase Separation in the Antiperovskite Nitride Mn_3ZnN

Ying Sun,[†] Cong Wang,*[,†] Qingzhen Huang,[‡] Yanfeng Guo,[§] Lihua Chu,[†] Masao Arai,[⊥] and Kazunari Yamaura*[,§]

[†]Center for Condensed Matter and Materials Physics, Department of Physics, Beihang University, Beijing 100191, P. R. China

[‡]NIST Center for Neutron Research, National Institute of Standards and Technology, Gaithersburg, Maryland 20899, United States

[§]Superconducting Properties Unit and [⊥]Computational Materials Science Center, National Institute for Materials Science, Tsukuba, Ibaraki 305-0044, Japan

Supporting Information

ABSTRACT: The antiperovskite Mn_3ZnN is studied by neutron diffraction at temperatures between 50 and 295 K. Mn_3ZnN crystallizes to form a cubic structure at room temperature (C1 phase). Upon cooling, another cubic structure (C2 phase) appears at around 177 K. Interestingly, the C2 phase disappears below 140 K. The maximum mass concentration of the C2 phase is approximately 85% (at 160 K). The coexistence of C1 and C2 phase in the temperature interval of 140−177 K implies that phase separation occurs. Although the C1 and C2 phases share their composition and lattice symmetry, the C2 phase has a slightly larger lattice parameter ($\Delta a \approx 0.53\%$) and a different magnetic structure. The C2 phase is further investigated by neutron diffraction under high-pressure conditions (up to 270 MPa). The results show that the unusual appearance and disappearance of the C2 phase is accompanied by magnetic ordering. Mn_3ZnN is thus a valuable subject for study of the magneto-lattice effect and phase separation behavior because this is rarely observed in nonoxide materials.

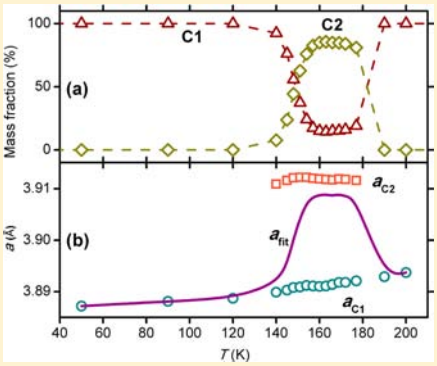

INTRODUCTION

Antiperovskite materials with the formula Mn_3XN (X = Ga, Zn, Cu, Ge, and Sn) have attracted significant attention in the past decade because of the discovery of some important phenomena such as their giant magnetoresistance,[1] near-zero temperature coefficient of resistivity,[2] and magnetostriction.[3] In addition, their associated crystallographic and magnetic properties make them promising materials for prospective uses in novel magnetoelectronic devices. Experimental evidence[4−8] has shown that complicated interactions between the lattice, the electronic freedom, and the spin carriers in Mn_3XN play a pivotal role in these phenomena.[9] However, many of the physical behaviors are still poorly understood. In particular, elucidation of the mechanism governing the tight relation between the lattice and the magnetic transitions has been a long-standing challenge. For the mechanism of this relation to be revealed in more detail, the remarkable strong coupling between the lattice and the magnetism in Mn_3XN should certainly be studied further.

The antiperovskite compound Mn_3ZnN has been investigated intensively in the past decade; Fruchart et al. reported in 1978 that two distinct magnetic transitions appear in Mn_3ZnN. Upon cooling, a paramagnetic state changes to an antiferromagnetic (AFM) state near 183 K with sudden lattice expansion. At 140 K, a sharp lattice contraction appears with further cooling, accompanied by another magnetic transition.[10] In 2001, Kim et al. observed only a single magnetic transition for Mn_3ZnN,[11] seemingly disagreeing with earlier observations. Recently, we found a resistive switching phenomenon for a high-pressure-synthesized dense pellet of Mn_3ZnN.[12] In order to shed more light on the relationship between the magnetic behavior and the lattice nature of Mn_3ZnN, we carried out a neutron diffraction study at low temperature and high pressure. As a result, we found that the complicated magnetic and structural transitions observed in Mn_3ZnN are strongly coupled and two cubic phases coexist in a certain temperature range, implying that phase separation (PS) occurs.

PS generally indicates that two or more distinct phases coexist in a thermodynamic state at a given temperature. Critical behavior usually results from the thermodynamic competition between phases with nearly identical free energies.[13] Such PS behaviors have been observed experimentally for various manganese and copper oxides such as $La_{1-x}Ca_xMnO_3$, $Pr_{1-x}Ca_xMnO_3$, and $La_{2-x}Sr_xCuO_4$.[14−16] In this paper, we present the results of a neutron diffraction study on Mn_3ZnN at low temperature and under high pressure. These results show a strong correlation between the lattice and the magnetism of two cubic phases that coexist in a single compound in the temperature range 140−177 K and at

Received: March 3, 2012
Published: June 21, 2012

   dx.doi.org/10.1021/ic300978x | Inorg. Chem. 2012, 51, 7232−7236

pressures below 250 MPa. PS, which is rarely observed for nonoxides, probably results from this correlation.

EXPERIMENTAL SECTION

A polycrystalline Mn_3ZnN sample was prepared through a solid-state reaction from fine powders of Mn_2N and Zn (99.99%), which were thoroughly mixed in a stoichiometric molar ratio. The precursor Mn_2N was prepared from Mn powder (99.99%) by heating at 800 °C for 60 h in nitrogen. The mixture was compressed into a pellet, then wrapped in tantalum foil, and heated in an evacuated quartz tube at 780 °C for 80 h.

High-resolution neutron powder diffraction (NPD) experiments were conducted in the BT-1 powder diffractometer at the NIST Center for Neutron Research using a monochromatic beam at λ = 1.5403 Å, produced with a Ge(311) monochromator. The Söller collimations before and after the monochromator and after the sample had full-width at half-maximum values of 15′, 20′, and 7′, respectively. The scan step was 0.05° in the 2θ range 10−165°. NPD data were collected at various temperatures between 50 and 295 K. The neutron-scattering amplitudes used in data analysis were −0.375, 0.568, and 0.936 ($\times 10^{-12}$ cm) for Mn, Zn, and N, respectively. The pressure effect on the NPD pattern was studied in the BT-1 instrument using an aluminum cell and helium gas as the pressure medium.[17] Atomic and magnetic structures were analyzed using the "General Structure Analysis System" (GSAS) program.[18]

The magnetic susceptibility (χ) of the loosely gathered powder of Mn_3ZnN was measured using a magnetic property measurements system, Quantum Design, at temperatures between 10 and 300 K in an applied magnetic field of 100 Oe. Magnetic hysteresis was measured in magnetic fields between −50 and 50 kOe at temperatures of 50 and 160 K.

RESULTS AND DISCUSSION

The NPD pattern of Mn_3ZnN measured at 295 K was analyzed by the Rietveld method (Figure 1). At the beginning, the

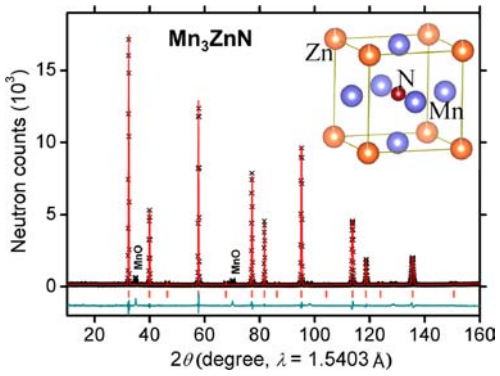

Figure 1. Rietveld analysis of the NPD pattern measured at room temperature for Mn_3ZnN. Cross markers and solid lines show the observed and calculated patterns, respectively; the difference is shown at the bottom. The positions of Bragg reflections are marked by ticks.

refinement was carried out by assuming that the space group was *Pm*-3*m* and all atomic sites for Zn, N, and Mn were fully occupied at 1*a* (0, 0, 0), 2*b* (0.5, 0.5, 0.5), and 3*c* (0, 0.5, 0.5), respectively. The solution indicated that the model can reasonably account for the NPD pattern for the present compound. Finally, we refined the pattern without fixing the occupancy factors for the Zn and N atoms. The occupancy factors of Mn, Zn, and N were refined to be 1 (fixed), 0.99(1), and 0.98(2), respectively, indicating that the atoms fully occupied each site. The lattice parameter of the cubic unit cell at room temperature was 3.90078(8) Å, and the unit-cell volume was 59.355(4) Å^3. The isotropic atomic displacement parameters were 0.0137(9) and 0.0124(6) Å^2 for Zn and N, respectively, while the anisotropic atomic displacement parameters for Mn were 0.0109(10), 0, 0, 0.0149(7), 0, and 0.0149(7) Å^2 for U_{11}, U_{12}, U_{13}, U_{22}, U_{23}, and U_{33}, respectively. The *R* factors of the final solution, R_{wp} and R_p, were 6.18% and 5.83%, respectively. A schematic crystal structure view based on the refined parameters is shown in the inset of Figure 1.

Next, we analyzed the patterns above 190 K using the cubic structure model as well, and the results indicated that the cubic structure with the space group of *Pm*-3*m* is reasonable. However, at temperatures between 177 and 140 K, additional lattice features such as peak splitting were visible in the NPD patterns. To highlight these features clearly, we show the temperature dependence of the *211* nuclear peak as a representative peak on the right side of Figure 2. This indicates

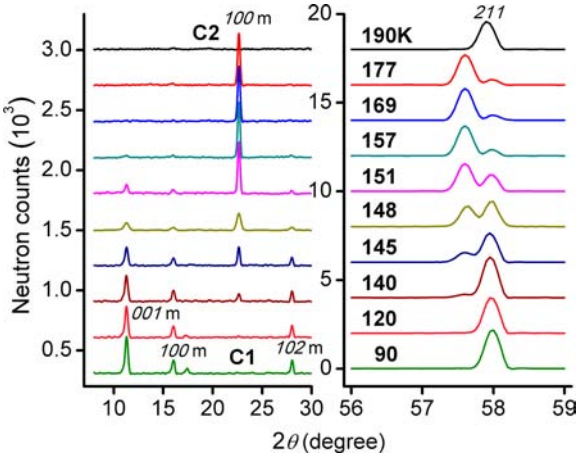

Figure 2. Thermal evolution of the NPD pattern: the *211* nuclear peak (right) and typical magnetic peaks (left) are shown. Note that the *100* magnetic peak at 177 K and below is from the C2 phase, while the *001*, *100*, and *102* peaks in the vicinity of 120 K are from the C1 phase.

that the peak splits into at least two peaks upon cooling and then goes back to a single peak when cooled further. Rietveld analysis of the NPD patterns indicated that the features were due neither to a structural transition nor to a symmetry change. The best fits to the observed NPD pattern at temperatures between 177 and 140 K were achieved by the two-cubic-phases model, in which there are two cubic lattices sharing the same space group but having slightly different lattice parameters. The NPD patterns measured at low temperatures (below 140 K) were rather better analyzed by the single-cubic-structure model than by the two-cubic-phases model.

The cubic phase that is stable at room temperature is herein referred to as C1; the other cubic phase that appears at temperatures between 177 and 140 K is called C2. The relative mass fraction between the C1 and the C2 phases was measured by Rietveld analysis and is plotted as a function of temperature in Figure 3a. The C2 fraction remains at zero down to 190 K and then rapidly rises to 80% at around 160 K. The C2 phase maintains a constant mass fraction in the temperature range between 150 and 180 K; however, at around 151 K it starts to decrease upon cooling and reaches zero again at 90 K and below. The lattice parameter of the C2 phase is nearly independent of temperature at a = 3.9114 (2) Å (see Figure 3b), which is approximately 0.53% larger than that of the C1 phase when compared at 160 K. Interestingly, the lattice

dx.doi.org/10.1021/ic300978x | Inorg. Chem. 2012, 51, 7232−7236

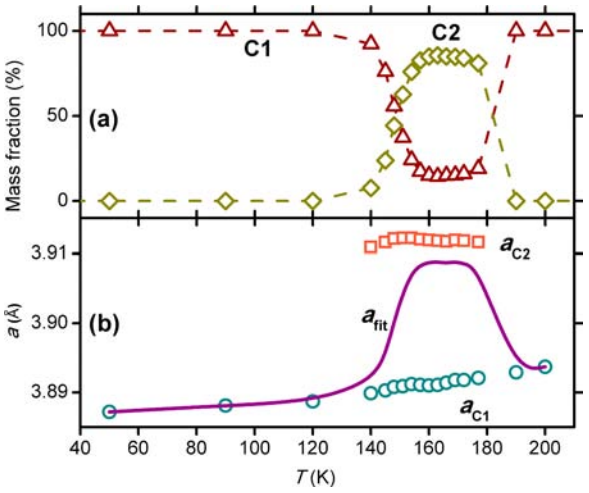

Figure 3. Temperature dependence of the (a) mass fraction and (b) cubic lattice parameter of Mn_3ZnN. Lattice parameter a_{fit} was calculated from the relation $a_{C1} \times f_{C1} + a_{C2} \times f_{C2}$, where f_{C1} and f_{C2} are the mass fractions of each phase.

parameter of the C2 phase points to a near zero thermal expansion coefficient of 8.65×10^{-7} K^{-1}, which is comparable to or slightly smaller than those of practical materials.[19]

As already shown in Figure 2, the thermal variation of the *211* nuclear peak is probably accompanied by development of the magnetic peaks. The *211* peak intensity is plotted as a function of temperature in Figure 4a (C1) and 4b (C2), along

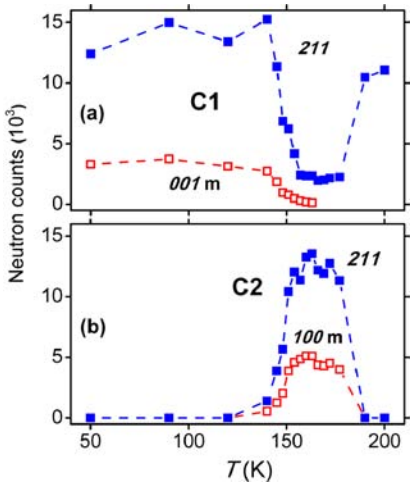

Figure 4. Temperature dependence of the (a) 211 nuclear peak and 001 magnetic peak intensities for the C1 phase and (b) 211 nuclear peak and 100 magnetic peak intensities for the C2 phase.

with the intensities of representative magnetic peaks. The plots clearly indicate that the appearance and disappearance of the C2 phase is coupled with development of the magnetic peaks. Both the nuclear and the magnetic peaks for the C2 phase appear simultaneously on cooling, and interestingly, the peaks disappear simultaneously with further cooling (see Figure 4b). In contrast, the magnetic peaks of the C1 phase appear at 151 K on cooling and are independent of the thermal evolution of the nuclear structure. In addition, the C1 phase maintains its magnetic structure down to 5 K, unlike in the situation observed for the C2 phase. The plots indicate that the magnetic and nuclear structures are strongly coupled with each other in the C2 phase.

The two magnetic structures of the C1 and C2 phases were analyzed using the magnetic structure models proposed for various Mn_3MX (M = metal and X = C or N) in 1978 by Fruchart and Bertaut.[10] The models used in this study are shown in the insets of Figure 5. The observed magnetic peaks

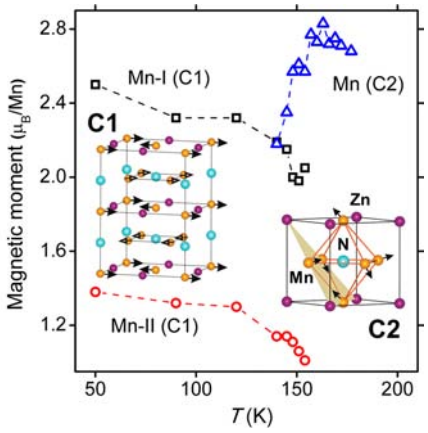

Figure 5. Ordered magnetic moments measured by neutron diffraction. (Insets) Magnetic structure models of the C1 (left) and C2 phases (right).[20] Arrows indicate the approximate directions of the magnetic moments at the Mn atoms.

were reasonably analyzed by these models; the estimated magnetic moment per Mn is plotted in Figure 5 as a function of temperature. In the C1 phase, two nonequivalent magnetic atoms Mn1 and Mn2 show an increase in the magnitude of each magnetic moment upon cooling, while the magnitude of the Mn moment in the C2 phase starts to decrease at 157 K on cooling. Note that the Mn moment of the C2 phase is slightly larger than that of the C1 phase.

In order to shed more light on the magnetic behavior, we measured the temperature dependence of χ in both cooling and warming cycles, as shown in Figure 6. The magnetic properties accord well with the results of the NPD measurements. The curves of χ versus T exhibit two peculiar features, which probably reflect the appearance and disappearance of the C2

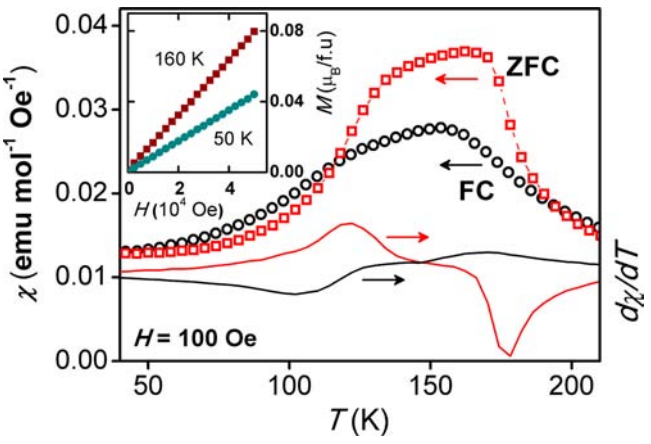

Figure 6. Temperature dependence of χ measured in an applied magnetic field of 100 Oe under both field-cooling (FC) and zero-field-cooling (ZFC) conditions. (Inset) M vs H curves measured at 50 and 160 K. Solid red and black curves at the bottom show dχ/dT vs T.

dx.doi.org/10.1021/ic300978x | Inorg. Chem. 2012, 51, 7232–7236

phase. Indeed, the AFM correlations were confirmed by the $M-H$ measurements at 50 and 160 K, as shown in the inset of Figure 6. The critical temperatures were estimated from the derivative curves of $d\chi/dT$ to be 178 and 121 K for the warming curve and 173 and 108 K for the cooling curve; thermal hysteresis indicates that there is a gap between the temperatures of appearance and disappearance of the C2 phase.

Let us now return to the results of the NPD study. The C2 phase coexists with the C1 phase in the temperature range 140−177 K. Because the C2 phase is accompanied by thermal hysteresis in the plot of χ versus T and the transport properties,[12] the C2 phase shows first-order-like appearance and disappearance behaviors. Thus, the C2 phase is probably a thermodynamic equilibrium state. A PS picture is therefore reasonable for the state in which the C1 and C2 phases coexist. If the state is not in thermal equilibrium, the C2 phase is supposed to be metastable, but the data obtained so far do not support the notion of a metastable C2 phase. The coincidence among neutron, magnetic, and resistivity data and the reversible change of PS behavior strongly suggest the stability of the C2 phase. Besides, our recent studies indicated that the C2 phase becomes stable even at the magnetic ground state when the materials are rich in Zn vacancies.[20]

The electronic structure of Mn_3XN has been studied by several groups. Narrow bands near the Fermi level (E_F) are formed because of the strong hybridization between the N 2p and Mn 3d orbitals, while X provides itinerant electrons at the Fermi energy.[10] A sharp singularity in the electronic density of states (DOS) lies very close to E_F.[21] The DOS structure thus tends to split into several singularities at different energy levels, with electron transfer from a high-energy level to a low-energy level within the p−d_{eg} subbands, leading to a large electronic contribution δF_e (electron free energy).[22]

Since the transferred electrons are lowered in energy, the contribution δF_e should be negative and hence is capable of inducing structural instability, as argued in ref 22. The electronic origin of the instability was also verified by heat-capacity measurements, which showed an anomalously higher electronic constant γ for the series of the antiperovskite Mn_3XN.[23] Moreover, either lattice or magnetic transitions are characterized well by discontinuities in γ over the transition temperatures. These observations are suggestive of a close relationship between the electronic structure instability and the PS in the antiperovskite Mn_3ZnN. Reports on both Mn_3XN and oxides suggest that PS is characteristic of strongly correlated systems, regardless of whether the compounds are oxide or nonoxide materials.

When a magnetic transition occurs in Mn_3XN, a large electronic contribution δF_e is expected. We therefore discuss PS in terms of the electronic stability condition $\kappa^{-1} = \langle n\rangle^2\delta^2F_e/\delta\langle n\rangle^2 > 0$, where κ is the electronic compressibility and n is the electron density. Derived from the formula $\kappa^{-1} \propto \partial\mu/\partial n$, where μ is the chemical potential, PS is closely related to the strength of interelectron interactions.[24] When $\partial\mu/\partial n < 0$, i.e., the chemical potential decreases with increasing electron density, the electronic state becomes thermodynamically unstable. The electronic state thus changes through PS to become lower energetically in order to maintain the thermodynamic equilibrium. A negative contribution to the electronic compressibility is thus capable of driving the PS. Generally, PS is an effect of the coupling between charged carriers and spins and the lattice. When the magnetic order plays a negligible role in varying the bandwidth, the compressibility should be proportional to the DOS at E_F.[25] The tendency toward PS is therefore accompanied by electronic anomalies caused by the magnetic transition.

Squeezing the lattice physically may provide an important verification of the above conjecture because the inhomogeneous electronic state may split into multiple states with different spin densities, and this process is thus expected to be highly sensitive to the applied pressure, as predicted theoretically for Mn_3GaN.[26] In addition, the sharp singularity in the DOS at E_F is usually affected by external parameters.[27] We therefore carried out high-pressure NPD measurements on Mn_3ZnN. In Figure 7a, the temperature dependences of the NPD intensity of the *211* peak for the C2 phase were measured at pressures of 0, 100, and 200 MPa. The applied pressure apparently reduces the *211* peak intensity, implying that the C2 phase becomes rather unstable under compressed conditions. Moreover, the transition temperature decreases almost linearly with increasing applied pressure; the ratio is roughly estimated to be −0.08 K/MPa, as depicted in the inset of Figure 7a.

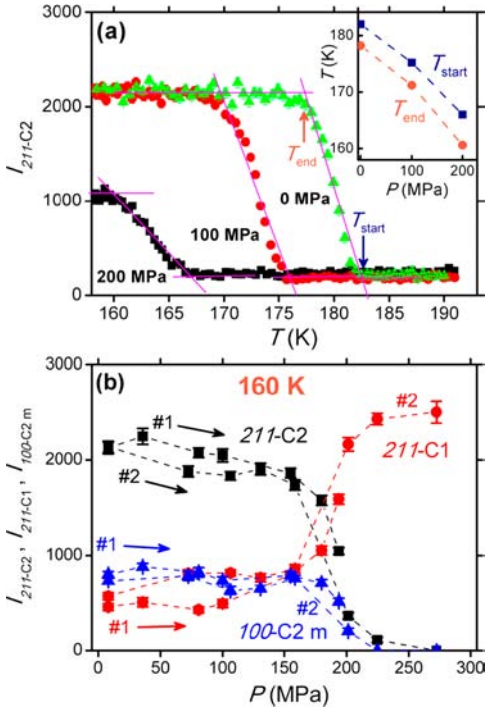

Figure 7. (a) Temperature dependence of the intensity of the *211* nuclear peak for the C2 phase under different applied pressures. (b) Pressure dependence of intensities of the *211* nuclear peaks and *100* magnetic peak measured at 160 K.

A decrease in phase-transition temperature upon application of pressure is often observed for itinerant-electron materials, mostly because the bandwidth is somewhat widened and the DOS at E_F decreases under pressure. In addition, the transition is broadened when the applied pressure increases. According to the argument by Iikubo et al. on a similar broadening recently observed for Ge-doped Mn_3CuN, local lattice distortion is primary responsible for this feature.[28] The broadened magnetic transition found for Mn_3ZnN under high-pressure conditions might be associated with a similar local lattice distortion. Further studies under these conditions may help to address this issue more fully.

dx.doi.org/10.1021/ic300978x | *Inorg. Chem.* 2012, 51, 7232−7236

The pressure dependences of the *211* nuclear and *100* magnetic peak intensities of the C2 phase were studied at 160 K (Figure 7b). It is notable that the peaks decrease sharply with increasing applied pressure and disappear at 250 MPa or higher. On the contrary, the *211* peak of the C1 phase increases with increasing applied pressure. The applied pressure probably suppresses the electronic instability and influences the electronic compressibility, leading to significant suppression of the PS. From another viewpoint, the denser phase of C1 becomes much more stable under compressed conditions than C2, which has a lower crystal density. The high-pressure study clearly revealed a close relationship between PS and the applied pressure.

The NPD results suggest that the two cubic phases are in close competition with each other. The C2 phase is highly susceptible to external conditions including temperature and pressure. In addition, on the basis of their theoretical study, Qu et al. predicted that N vacancies in the lattice have a significant influence on the competition between the two cubic phases in Mn_3ZnN.[29] It is difficult to control the N vacancies during synthesis, so this may account for the large variations in experimental results for Mn_3ZnN.[30] Besides, Zn vacancies also play a major role in terms of the thermodynamic stability of the two cubic phases in Mn_3ZnN.[20] Further investigations on the effect of nonstoichiometry are underway.

CONCLUSIONS

In summary, the unusual phase separation of the antiperovskite Mn_3ZnN was studied by NPD under high-pressure conditions. The temperature and pressure dependences of the NPD peaks showed that two cubic phases coexist in the temperature interval $140 \leq T \leq 177$ K and at pressures below 250 MPa. The results indicated that there is a close correlation between the lattice and magnetic ordering. Surprisingly, the ground state is dominated only by a single cubic phase. The unusual appearance and disappearance of the cubic phase in a particular $P-T$ range was argued to be due to a PS, which is rarely observed for nonoxide materials. Although the exact mechanism of PS in Mn_3ZnN is still under discussion, it is probable that the electronic contribution to the free energy accounts for the unusual behavior. Further theoretical consideration focusing on Mn_3ZnN is necessary for a comprehensive picture of the exact mechanism to be obtained.

ASSOCIATED CONTENT

Supporting Information

Neutron diffraction patterns at different temperatures. This material is available free of charge via the Internet at http://pubs.acs.org.

AUTHOR INFORMATION

Corresponding Author

*E-mail: congwang@buaa.edu.cn (C.W.); yamaura.kazunari@nims.go.jp (K.Y.).

Notes

The authors declare no competing financial interest.

ACKNOWLEDGMENTS

We acknowledge the support of the National Institute of Standards and Technology, U.S. Department of Commerce, in providing the neutron research facilities used in this work. This work was financially supported by the National Natural Science Foundation of China (NSFC) (91122026 and 51172012), the World Premier International Research Center from MEXT (Japan), a Grant-in-Aid for Scientific Research (22246083) from JSPS (Japan), the Funding Program for World-Leading Innovative R&D on Science and Technology (FIRST Program) from JSPS (Japan), and the Advanced Low Carbon Technology Research and Development Program (ALCA) from JST (Japan).

REFERENCES

(1) Kamishima, K.; Goto, T.; Nakagawa, H.; Miura, N.; Ohashi, M.; Mori, N.; Sasaki, T.; Kanomata, T. *Phys. Rev. B* **2000**, *63*, 024426.
(2) Sun, Y.; Wang, C.; Chu, L. H.; Wen, Y. C.; Nie, M.; Liu, F. S. *Scr. Mater.* **2010**, *62*, 686.
(3) Asano, K.; Koyama, K.; Takenaka, K. *Appl. Phys. Lett.* **2008**, *92*, 161909.
(4) Mekata, M. *J. Phys. Soc. Jpn.* **1962**, *17*, 796.
(5) Iikubo, S.; Kodama, K.; Takenaka, K.; Takagi, H.; Takigawa, M.; Shamoto, S. *Phys. Rev. Lett.* **2008**, *101*, 205901.
(6) Song, B.; Jian, J. K.; Bao, H. Q.; Lei, M.; Li, Hui.; Wang, G.; Xu, Y. P.; Chen, X. L. *Appl. Phys. Lett.* **2008**, *92*, 192511.
(7) Bertaut, E. F.; Fruchart, D. *Solid State Commun.* **1968**, *6*, 251.
(8) Lord, J. S.; Armitage, J. G. M.; Riedi, P. C.; Matart, S. F.; Demazeaui, G. *J. Phys: Condens. Matter* **1994**, *6*, 1779.
(9) Kim, W. S.; Chi, E. O.; Kim, J. C.; Choi, H. S.; Hur, N. H. *Solid Sate Commun.* **2001**, *119*, 507.
(10) Fruchart, D.; Bertaut, E. F. *J. Phys. Soc. Jpn.* **1978**, *44*, 781.
(11) Kim, W. S.; Chi, E. O.; Kim, J. C.; Hur, N. H.; Lee, K. W.; Choi, Y. N. *Phys. Rev. B* **2003**, *68*, 172402.
(12) Sun, Y. S.; Guo, Y. F.; Wang, X. X.; Tsujimoto, Y.; Matsushita, Y.; Shi, Y. G.; Wang, C.; Belik, A. A.; Yamaura, K. *Appl. Phys. Lett.* **2012**, *100*, 161907.
(13) Granado, E.; Huang, Q.; Lynn, J. W.; Gopalakrishnan, J.; Greene, R. L.; Ramesha, K. *Phys. Rev. B* **2002**, *66*, 064409.
(14) Moritomo, Y.; Kuwahara, H.; Tomioka, Y.; Tokura, Y. *Phys. Rev. B* **1997**, *55*, 7549.
(15) Bozin, E. S.; Kwei, G. H.; Takagi, H; Billinge, S. J. L. *Phys. Rev. Lett.* **2000**, *84*, 5856.
(16) Huang, Q.; Lynn, J. W.; Erwin, R. W.; Santoro, A.; Dender, D. C.; Smolyaninova, V. N.; Ghosh, K.; Greene, R. L. *Phys. Rev. B* **2000**, *61*, 8895.
(17) dela Cruz, C. R.; Lorenz, B.; Ratcliff, W.; Lynn, J.; Gospodinov, M. M.; Chu, C. W. *Physica B* **2008**, *403*, 1359.
(18) Larson, A. C.; Von Dreele, R. B. *Los Alamos National Laboratory Report LAUR* **2000**, *86*, 748.
(19) Takenaka, K. *Sci. Technol. Adv. Mater.* **2012**, *13*, 013001.
(20) Wang, C.; Chu, L. H.; Yao, Q. R.; Sun, Y.; Wu, M. M.; Ding, L.; Yan, J.; Na, Y. Y.; Tang, W. H.; Li, G. N.; Huang, Q.; Lynn, J. W. *Phys. Rev. B* **2012**, *85*, 220103(R).
(21) Garcia, J.; Bianconi, A.; Marcelli, A.; Davoli, I.; Bartolome, J. *IL Nuovo Cimento* **1986**, *7D*, 493.
(22) Jardin, J. P.; Labbe, J. *J. Solid State Chem.* **1983**, *46*, 275.
(23) García, J.; Bartolomé, J.; González, D.; Navarro, R.; Fruchart, D. *J. Chem. Thermodyn.* **1983**, *15*, 465.
(24) Arovas, D. P.; Santos, G. G.; Guinea, F. *Phys. Rev. B* **1999**, *59*, 13569.
(25) Guinea, F.; Santos, G. G.; Arovas, D. P. *Phys. Rev. B* **2000**, *62*, 391.
(26) Lukashev, P.; Sabirianov, R. F.; Belashchenko, K. *Phys. Rev. B* **2008**, *78*, 184414.
(27) Kaneko, T.; Kanomata, T.; Shirakawa, K. *J. Phys. Soc. Jpn.* **1987**, *56*, 4047.
(28) Iikubo, S.; Kodama, K.; Takenaka, K.; Takagi, H.; Takigawa, M.; Shamoto, S. *Phys. Rev. Lett.* **2008**, *101*, 205901.
(29) Qu, B. Y.; Pan, B. C. *J. Appl. Phys.* **2010**, *108*, 113920.
(30) Sun, Y.; Wang, C.; Wen, Y. C.; Zhu, K. G.; Zhao, J. T. *Appl. Phys. Lett.* **2007**, *91*, 231913.